International Journal of Modern Physics B
Vol. 31 (2017) 1740005 (14 pages)

DOI: 10.1142/S0217979217400057

On the origin of nonlocal damping in plasmonic monomers and dimers

Christos Tserkezis*
Department of Photonics Engineering, Technical University of Denmark, DK-2800 Kongens Lyngby, Denmark
ctse@fotonik.dtu.dk

Wei Yan
Laboratoire Photonique, Numérique et Nanosciences (LP2N), IOGS Univ. Bordeaux CNRS, 33400 Talence cedex, France

Wenting Hsieh
Department of Physics, University of Massachusetts, Boston, Massachusetts 02125, USA

Greg Sun
Department of Engineering, University of Massachusetts, Boston, Massachusetts 02125, USA

Jacob B. Khurgin
Department of Electrical and Computer Engineering, Johns Hopkins University, Baltimore, Maryland 21218, USA

Martijn Wubs
Department of Photonics Engineering, Technical University of Denmark, DK-2800 Kongens Lyngby, Denmark
Center for Nanostructured Graphene, Technical University of Denmark, DK-2800 Kongens Lyngby, Denmark
mwubs@fotonik.dtu.dk

N. Asger Mortensen*
Center for Nano Optics, University of Southern Denmark, Campusvej 55, DK-5230 Odense M, Denmark
Center for Nanostructured Graphene, Technical University of Denmark, DK-2800 Kongens Lyngby, Denmark
Department of Photonics Engineering, Technical University of Denmark, DK-2800 Kongens Lyngby, Denmark
asger@mailaps.org

*Corresponding authors.

Received 3 March 2017
Revised 2 May 2017
Accepted 16 May 2017
Published 18 July 2017

The origin and importance of nonlocal damping is discussed through simulations with the generalized nonlocal optical response (GNOR) theory, in conjunction with time-dependent density functional theory (TDDFT) calculations and equivalent circuit modeling, for some of the most typical plasmonic architectures: metal–dielectric interfaces, metal–dielectric–metal gaps, spherical nanoparticles and nanoparticle dimers. It is shown that diffusive damping, as introduced by the convective–diffusive GNOR theory, describes well the enhanced losses and plasmon broadening predicted by *ab initio* calculations in few-nm particles or few-to-sub-nm gaps. Through the evaluation of a local effective dielectric function, it is shown that absorptive losses appear dominantly close to the metal surface, in agreement with TDDFT and the mechanism of Landau damping due to generation of electron–hole pairs near the interface. Diffusive nonlocal theories provide therefore an efficient means to tackle plasmon damping when electron tunneling can be safely disregarded, without the need to resort to more accurate, but time-consuming fully quantum-mechanical studies.

Keywords: Nonlocal optical response; plasmon damping; convective–diffusive theory.

PACS numbers: 78.67.Bf, 73.20.Mf, 72.10.Fk

1. Introduction

Following the advances in nanofabrication, the research field of plasmonics has developed on the foundation of classical electrodynamics and semiclassical descriptions of light–matter interactions.[1–3] In most cases, the collective oscillations of free electrons subject to optical fields are conceptually analyzed within the Drude theory,[4] inherently using the local-response approximation (LRA). Within this picture, the material response occurs only at the spatial position of the perturbation, while there is not even the slightest response at any short range away.[5] For dielectric media, this is a well-established and accurate approach, while metals in principle support short-range correlations that are potentially important to true nanoscale plasmonics and applications in the field of quantum plasmonics.[6–9] Despite its simplifications, the LRA framework has fostered both theory predictions and experimental confirmations of a large range of plasmonic phenomena, such as confining of light beyond the diffraction limit[10,11] and tuning the optical properties of metallic architectures through size and shape variations.[12] Large enhancement of electric fields in the vicinity of metal nanostructures[13–15] is another interesting plasmonic property, where abrupt variations in metal-surface topology may support huge amplifications. Such field enhancement is intimately linked to field singularities, which are inherent to LRA.

Accounts of light–matter interactions commonly rely on linear-response theory. For dielectric materials, the further simplification associated with LRA usually holds all the way down to the atomic scale. The success of LRA is in some way more intriguing in the case of nanoplasmonics. On the one hand, experimental characterization of gold dimers with narrow, few-nm gaps has been found to agree

well with classical electrodynamics.[16] On the other hand, when light interacts with the free electrons in metals, the optical response is anticipated to exhibit a nonlocal character, with the corresponding response function becoming spatially dispersive.[5]

The underlying quantum wave dynamics of the electron gas manifests itself at a length scale intrinsic to the metal: the Fermi-wavelength scale. For most metals, this lies in the nanometer-to-Angstrom scale regime.[4] Such a small scale can therefore justify the success of LRA and the application of Drude theory to plasmonics even in nanoscale metallic structures. At the same time, it also hints to the mesoscopic size regime for which a departure from the predictions of classical electrodynamics can be anticipated. This expectation has been confirmed, for example, for arbitrarily sharp changes in the metal-surface topography and in dimers with vanishing gaps, where disregarding nonlocality causes the field to diverge within the LRA response.[15,17]

Here, we review the aspects of the nonlocal response of metallic nanoparticles, which were recently revived[18–21] by the realization of state-of-the-art experiments on plasmonics in structures of ever smaller dimensions.[22–31] In particular, we first explore the real-space formulation[21,32] and numerical implementations[33] of the long-existing nonlocal hydrodynamic theory.[34–37] We then address a recent extension of this theory which accounts for drift–diffusion dynamics, namely the generalized nonlocal optical response (GNOR) theory.[38] By extracting an effective local dielectric function of the metal from GNOR simulations, and in comparison with time-dependent density functional theory (TDDFT) calculations for metal–dielectric interfaces, we show that the increased plasmon damping in small nanoparticles and narrow gaps can be fully understood in terms of induced-charge diffusion, thus providing a connection between Landau damping and the nonlocal optical response.[39–42]

2. Nonlocal Electrodynamics

Theoretical modeling of plasmonic phenomena widely relies on the macroscopic Maxwell's equations.[1] Here, the optical response of metals is described through constitutive relations connecting the response of the material to the applied field. In particular, the displacement field $\mathbf{D}$ generated at a point $\mathbf{r}$ in response to a perturbing electric field $\mathbf{E}$ is in general given by the nonlocal constitutive relation

$$\mathbf{D}(\omega, \mathbf{r}) = \varepsilon_0 \int d\mathbf{r}' \varepsilon(\omega, \mathbf{r}, \mathbf{r}') \mathbf{E}(\omega, \mathbf{r}'), \tag{1}$$

where ε_0 is the vacuum permittivity, ω is the angular frequency of light and ε is the corresponding (nonlocal) permittivity of the metal. Introducing Eq. (1) into Maxwell's equations, one arrives at the integro-differential wave equation

$$\nabla \times \nabla \times \mathbf{E}(\omega, \mathbf{r}) = \left(\frac{\omega}{c}\right)^2 \int d\mathbf{r}' \varepsilon(\omega, \mathbf{r}, \mathbf{r}') \mathbf{E}(\omega, \mathbf{r}'), \tag{2}$$

where c is the velocity of light in vacuum. The above equation is not particularly appealing, as it is not straightforward to solve it, either analytically or numerically.

However, if one focuses on short-range correlations, it can be transformed into a regular partial differential equation[32,38,43]

$$\nabla \times \nabla \times \mathbf{E}(\omega, \mathbf{r}) = \left(\frac{\omega}{c}\right)^2 \left[\varepsilon_{\mathrm{LRA}}(\omega) + \xi^2 \nabla(\nabla \cdot)\right] \mathbf{E}(\omega, \mathbf{r}). \tag{3}$$

Here, ξ gives the range for the nonlocal response, while $\varepsilon_{\mathrm{LRA}}$ is the usual Drude contribution. Within GNOR hydrodynamics, the nonlocal length scale is given by[38]

$$\xi^2 = \frac{\beta^2}{\omega(\omega + i\gamma)} + \frac{D}{i\omega}, \tag{4}$$

where $\beta^2 = 3/5 v_F^2$ with v_F being the Fermi velocity, while $D \propto v_F^2 \tau$ is a diffusion constant associated with impurity scattering, τ is the free-electron relaxation time, and $\gamma = 1/\tau$ is the usual Drude damping rate.[32,38] Setting $D = 0$ in Eq. (4), one immediately retrieves the standard nonlocal hydrodynamic Drude model (HDM), which predicts modal blueshifts, but no additional broadening.[32]

To get more physical insight into the role of the diffusion term in the hydrodynamic description of the electron gas, the relaxation dynamics has to be considered. Under the influence of an external electric field, the free electrons in an initially charge-neutral metallic nanostructure are drawn away from their equilibrium positions, leaving regions near the surfaces with excess and deficit densities of charge, i.e., an induced net surface charge. At the same time, of course, the bulk remains uncharged, since the positive ions remain fully screened by a corresponding density of negatively charged conduction electrons. As a consequence of entropy, the induced spatially inhomogeneous charge density will relax towards its equilibrium distribution, a relaxation driven by surface scattering and many-body electron–electron interactions. Classically, this is described as diffusion and in a drift–diffusion theory, this is captured by the diffusion constant D. Since diffusion relaxes the induced charge, it also relaxes the polarization field, and consequently it is a damping mechanism.

3. Bridging the Nonclassical Response of Monomers and Dimers

Individual metallic nanoparticles, and their dimer counterparts, constitute the archetypal plasmonic structures. In the following, we show that GNOR is versatile enough to offer an understanding of the enhanced damping mechanisms in both. Several attempts to tackle this issue have been presented over the years. Among the pioneers, Kreibig and co-workers presented a phenomenological model (referred to as SDB in what follows) which successfully captures the size-dependent spectral broadening observed in few-nm, nearly-spherical nanoparticles.[44] Apart from its phenomenological character, the main disadvantage of this approach is the absence of simple guidelines on how to apply it to nonspherical monomers or to strongly interacting dimers composed of particles that are not necessarily small themselves. In a recent effort to deal with nonclassical effects in dimers, Esteban *et al.* developed a quantum-corrected model,[45] which introduces quantum tunneling as the

main driving force behind the dimer nonclassical optical response. Tunneling-based theories, however, cannot naturally address the nonclassical aspects of the optical response of the corresponding monomers. This is where GNOR proves to be versatile and with a predictive power reaching far beyond either of the limiting cases described above. Despite its simplicity and semiclassical nature, GNOR provides a unified description of both size-dependent damping in monomers and gap-dependent broadening in dimers, and stresses the connection between the two, simply through the addition of a diffusive term to standard hydrodynamics.

Let us first briefly discuss the case of a monomer. We consider a metallic nanosphere of radius R, for which the complex-valued nonlocal length scale ξ in Eq. (4) leads to $1/R$ corrections to both the dipole resonance frequency and to its linewidth.[38] This observation provides an immediate link between the diffusion constant D and the A coefficient appearing in the approach developed by Kreibig *et al.*,[44] in which the Drude damping rate γ is corrected by adding the term Av_F/R. For most metals, A is experimentally found to be of order unity. This plasmon broadening, and the way it is captured by the SDB and GNOR models, is schematically depicted in Fig. 1, where we show typical extinction spectra for a few-nm metallic nanoparticle within the LRA, SDB, HDM and GNOR models. A more detailed description of the differences between the four models and their application to different types of metals and statistical ensembles of small, weakly interacting nanoparticles can be found in Ref. 46.

In a similar manner, it has also been shown that the very same choice of the diffusion constant D can qualitatively explain the gap-dependent broadening of spectra for dimers as well.[38] So, what is the important common feature of monomers and dimers? Can the experimentally observed broadening[24,47] be attributed exclusively

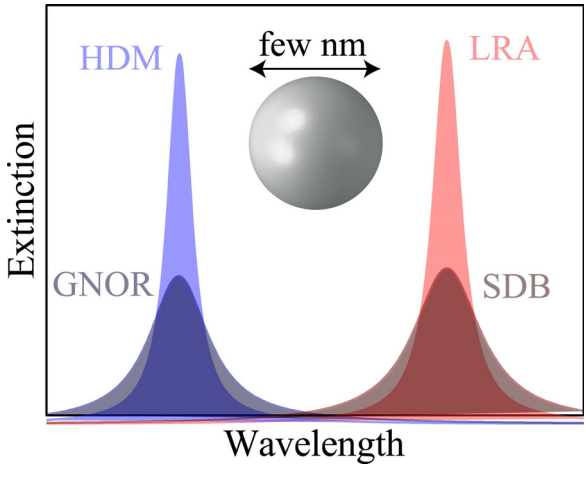

Fig. 1. (Color online) Schematic representation of typical extinction spectra calculated within the LRA (light red), SDB (dark red), HDM (light blue), and GNOR (dark blue) models, for a few-nm plasmonic nanosphere.

to a short-circuiting of the capacitive junction due to tunneling — as described in the quantum-corrected model[45] and its more recent extensions?[48,49] Or could diffusive damping — for which we will give a microscopic explanation below — account for it? Of course, there is no reason why these mechanisms could not co-exist and act simultaneously.

To facilitate a qualitative discussion, we employ a circuit model that addresses the relative importance of diffusive damping (characterized by a resistance $R_{\rm dif}$) and the damping associated with the relaxation of the quantum tunneling current (characterized by $R_{\rm tun}$) short-circuiting the classically impenetrable capacitive gap (characterized by a capacitance C). Within this equivalent circuit model, C and $R_{\rm tun}$ are connected in parallel to describe the plasmonic gap[50,51] and this branch is then connected in series with $R_{\rm dif}$. The equivalent impedance is given by

$$Z = R_{\rm dif} + \frac{R_{\rm tun}}{1 + i\omega\tau_{\rm tun}} = R_{\rm dif} - \frac{i}{\omega C} + \mathcal{O}[1/(\omega\tau_{\rm tun})^2], \tag{5}$$

where $\tau_{\rm tun} = R_{\rm tun}C$ is interpreted as the tunneling RC time.[50] This RC model has been successful in analyzing the ultra-fast response of a scanning-tunneling microscope.[50] Here, we extended it to include the dissipation associated with the diffusive dynamics.

The tunneling dynamics simplifies in the slow adiabatic-following regime and the limit of fast external driving.[52] The high-frequency dimer dynamics is therefore entirely dominated by the diffusive broadening and the junction capacitance, see the second equality in Eq. (5). In the context of the mesoscopic capacitance,[53] ultra-fast tunneling experiments have reported tunneling RC times that lie in the picosecond range,[50,54] implying that at optical frequencies, the plasmon response may just be too fast. If this is the case, $\omega\tau_{\rm tun} \gg 1$, and the relaxation will be dominated by diffusive broadening.

The above circuit analysis does not depend on the exact tunneling mechanism. Whethersana tunneling relaxation occurs within the gap, as assumed in the quantum-corrected model,[45] or inside the metal surfaces, as in the model by Hohenester[49] (in agreement with the common understanding of relaxation processes in mesoscopic quantum electron transport), is not relevant here, and the conclusions are unaltered. Nevertheless, it should be stressed that, given the qualitative nature of the above analysis and the lack of conclusive data for the RC time in plasmonic dimers, the situation still remains open. In fact, for few-Angstrom gaps, a different shorter RC time might be reasonable, in which case tunneling shall indeed become important.[42,55]

4. Connection Between Diffusion and Landau Damping

The SDB correction introduced by Kreibig *et al.* has already been linked to quantum mechanical calculations of Landau damping associated with surface-enhanced electron–hole pair generation in the metal.[39,56,57] More recently, *ab initio* studies[42] and electron spectroscopy[30,58,59] have established plasmon damping exceeding the

expectations based on bulk material parameters at the very surface of metals. The underlying many-body interaction within the electron gas is captured by GNOR with one single and entirely classical parameter: the diffusion constant D. Since the induced charge resides near the metal surface, this is where diffusion is also effective, as it is shown by the nonlocal correction term in Eq. (3), which mainly contributes near the surface where the **E** field changes the most. This is why our drift–diffusion model mimics both longitudinal pressure waves and Landau-like damping so well. The enhanced damping near the surface is illustrated in Fig. 2 where we show the local effective permittivity $\varepsilon_{\mathrm{eff},x}(\mathbf{r},\omega)$ (the component normal to the metal–air interface, x-axis) extracted from GNOR simulations ($\gamma = 0.0023\omega_p$, $v_F = 0.0045c$, $D = 2\omega_p/c^2$) via $\mathbf{D}(\mathbf{r},\omega) \equiv \varepsilon_0\varepsilon_{\mathrm{eff}}(\mathbf{r},\omega)\mathbf{E}(\mathbf{r},\omega)$, for either a flat metal–air interface (a) or a narrow metal–air–metal cavity (b). It is important to note here that, due to the abrupt termination of the surface and the associated hard-wall boundary condition for the normal component of the current, the additional damping occurs

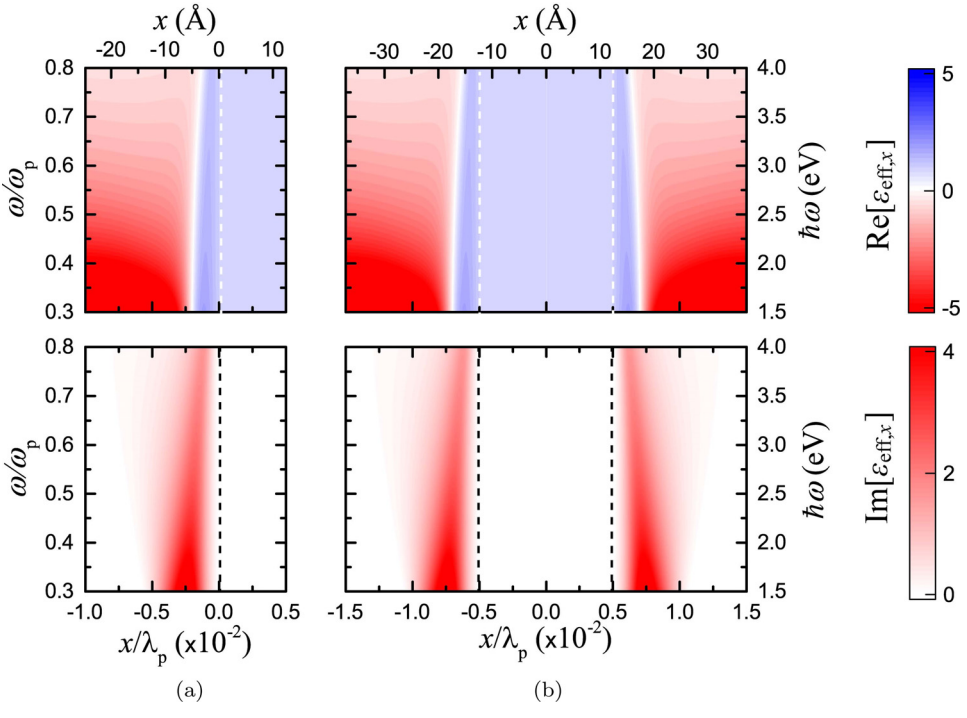

Fig. 2. (Color online) GNOR results for the real part (top panels) and imaginary part (lower panels) of $\varepsilon_{\mathrm{eff},x}$ (where x corresponds to the direction normal to the interface) for different frequencies (normalized to the metal plasma frequency ω_p) throughout the optical range, as a function of distance x (normalized to the plasma wavelength $\lambda_p = 2\pi c/\omega_p$). (a) A single metal–air interface with an infinite work function and a homogeneous equilibrium electron density that vanishes abruptly outside the metal surface. (b) Corresponding metal–air–metal cavity with a 0.01 λ_p gap separating the two surfaces. Right and top axis scales give the corresponding values in energy and length, assuming a plasma energy $\hbar\omega_p = 5$ eV. Dashed lines denote the metal–air interfaces.

slightly inside the surface. This links up to the Feibelman parameter[60] and its associated quantum corrections to electrodynamics.[61] The importance of relaxing the hard-wall boundary condition and considering the actual position of the surface of the electron plasma was recently discussed by Teperik and co-workers[62,63] in the context of plasmonic ruler effects of sub-nm gap dimers. In the spirit of our current discussion, it has recently been shown that density-gradient and spill-out effects can also be included in self-consistent hydrodynamic models.[64–66]

The role of Landau damping for both monomers and dimers can be pictorially illustrated by the time-dependent optical response of the electron gas near the surface of the metal.[42] We consider a simple metal, such as Na, described within a jellium approximation, and exploit TDDFT to obtain its response to a time-dependent electrical field.[42,62] The calculation provides both the (space-dependent) equilibrium density $n_0(\mathbf{r})$ and the induced charge density $n_1(\mathbf{r})$. Additionally, one also obtains the displacement field $\mathbf{D}$ generated by the perturbing $\mathbf{E}$ field, and from this, one may again infer an effective relative dielectric function $\varepsilon_{\text{eff}}(\mathbf{r},\omega)$, where the imaginary part holds key information about damping and its spatial localization. The top panel of Fig. 3(a) illustrates the equilibrium density (exhibiting both Friedel oscillations and quantum spill-out) along with the real part (middle panel) and imaginary part (lower panel) of $\varepsilon_{\text{eff},x}$ as a function of frequency. Observing the imaginary part of $\varepsilon_{\text{eff},x}$, one can immediately note how large Landau damping (exceeding the bulk damping) takes place in the near vicinity of the surface. We also note that this large imaginary part of $\varepsilon_{\text{eff},x}$ is always accompanied by a change in sign for the real part, which denotes the presence of a metal–dielectric interface, and is the prerequisite for plasmon excitation. In addition, we note that the large imaginary part regularizes the field enhancement driven by the vanishing real part, as first explored by Öztürk *et al.*[67]

The same calculation can be done for dimers as well. In the one-dimensional example studied above, this corresponds to two opposing jellium surfaces separated only by a sub-nm gap. The corresponding calculation for a 0.5-nm gap is shown in Fig. 3(b), where we recover the physical picture obtained for the single interface. Significant Landau damping occurs now at both interfaces, while there is no appreciable damping inside the gap. In fact, the response of the dimer is well represented by a simple superposition of the response of two opposing independent surfaces, see Fig. 3(c), thus confirming the suggestion of the circuit analysis: even for a gap of 0.5 nm, the dissipation is dominated by Landau damping, and tunneling currents do not change the plasmon-energy dissipation. We note that the typical *ab initio* simulations of the electron–gas dynamics include no energy-relaxation processes (e.g., coupling to a thermalizing phonon bath) and as such tunneling currents are necessarily relaxed only through the generation of electron–hole pairs. We emphasize that the observed importance of Landau damping does not rule out the existence of quantum tunneling currents at optical frequencies; in the present context of 0.5-nm gaps, such currents start to appear, but they do not significantly

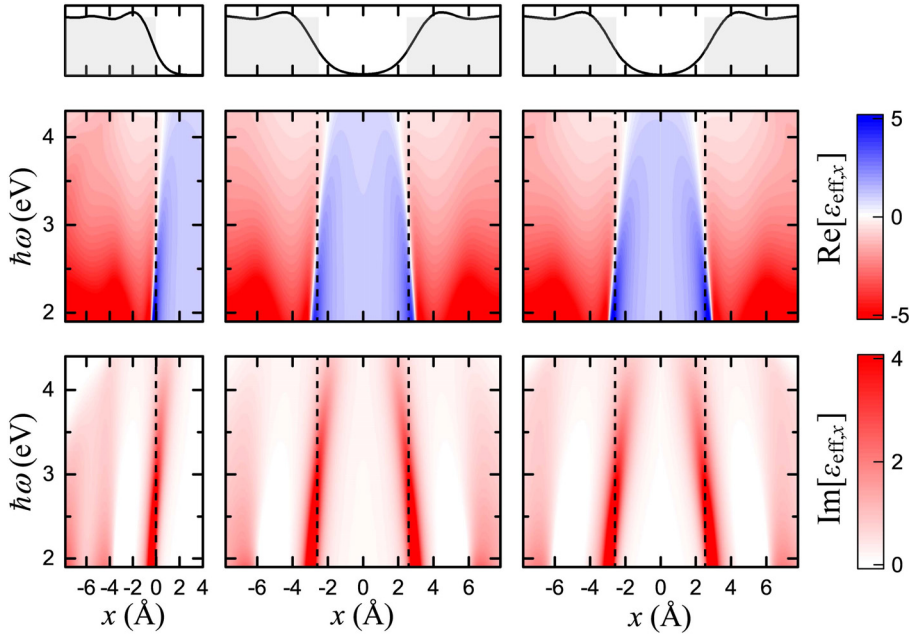

Fig. 3. (Color online) Equilibrium density in the jellium model (top panels), exhibiting both Friedel oscillations and electron spill-out, along with the TDDFT results for the real part (middle panels) and imaginary part (lower panels) of $\varepsilon_{\mathrm{eff},x}$ as a function of frequency. (a) A single Air–Na interface. (b) Full TDDFT calculation for two interacting Na surfaces separated by a 0.5-nm air gap. (c) The same metal–air–metal gap as in (b), with the results obtained by a superposition of two of the independent surfaces shown in (a). All contours share a common color scale.

influence the gap-dependent broadening of dimers yet. One needs to enter the true Angstrom-scale regime, where the individual atoms start to matter.

To further advance our description, we shift attention from flat interfaces to single metallic nanoparticles. In addition to the methods described above, the effective dielectric function can also be calculated by adding up in the Drude expression the bulk (γ_b) and surface broadening damping rate [$\gamma_s(r)$], according to Matthiesen's rule as[41]

$$\varepsilon(r) = \varepsilon_b - \frac{\omega_p^2}{\omega^2 + i\omega\left[\gamma_s(r) + \gamma_b\right]}, \tag{6}$$

where ε_b is the background dielectric constant. The surface collision damping and spectral broadening γ_s can be viewed as originating from direct transitions between two free-electron states near the Fermi level in the metal, enabled by the collision with a metal wall, which would otherwise be prohibited by the momentum conservation requirement. In that respect, a collision with the metal surface is considered to be no different from any other collision, with say, a phonon or a defect. The transition rate has been estimated using extended-in-momentum

(k)-space wavefunctions and a wavevector-dependent Lindhard dielectric function, as described in Refs. 40 and 68. Applying the inverse Fourier transform to these results, one can obtain the spatial distribution of the transition rate, and then the position-dependent effective dielectric constant, as follows from the consideration outlined below. When the plasmon polariton gets absorbed, the electrons (holes) get excited in the wide energy range from the Fermi level E_F to $E_F + \hbar\omega$, i.e., in the wave vector range from k_F (the Fermi wavenumber) to about $k_F + \omega/v_F$. Due to the boundary condition at the surface, all the wavefunctions are in phase and form a wave packet with a full-width at half-maximum of roughly $\Delta L \simeq \pi v_F/\omega = \lambda v_F/(2c)$, or about 0.7 nm for $\lambda = 370$ nm. The shape of the position-dependent absorption $\gamma_s(r)$ obviously follows the shape of the excited wave packet, which leads to the effective dielectric function of Eq. (6) exhibiting a spatial dependence, as shown in Fig. 4 for an $R = 5$ nm Drude nanosphere ($\varepsilon_b = 4.1$, $\hbar\omega_p = 9.3$ eV, $\hbar\gamma_b = 0.013$ eV, and $\hbar\gamma_s$ relaxing at 0.83 eV[41]). One indeed observes a very strong dependence for the imaginary part, and much less pronounced for the real part.

To further explore nonlocal damping in plasmonic nanostructures, we now turn to noble metals, and study in Fig. 5 the case of an Ag nanosphere dimer in air, using the implementation of the GNOR model[69] to a commercial finite-element solver (Comsol Multiphysics 5.0).[70] Silver is described here by a Drude model, with the core-electron part of the dielectric function obtained from the experimental dielectric function of Johnson and Christy,[71] as described in Ref. 46. The two spheres, of radius $R = 5$ nm, are separated by a 2-nm gap, and illuminated by

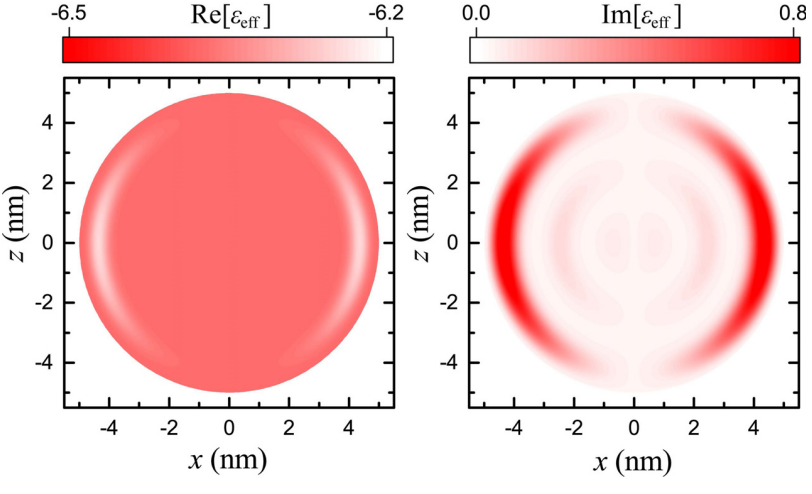

Fig. 4. (Color online) Real (left-hand contour) and imaginary (right-hand contour) part of the effective dielectric function, $\varepsilon_{\rm eff}$, calculated at the resonant wavelength ($\lambda = 370$ nm) for a Drude nanosphere ($\varepsilon_b = 4.1$, $\hbar\omega_p = 9.3$ eV, $\hbar\gamma_b = 0.013$ eV, $\hbar\gamma_s = 0.83$ eV) of radius $R = 5$ nm, calculated according to Eq. (6).

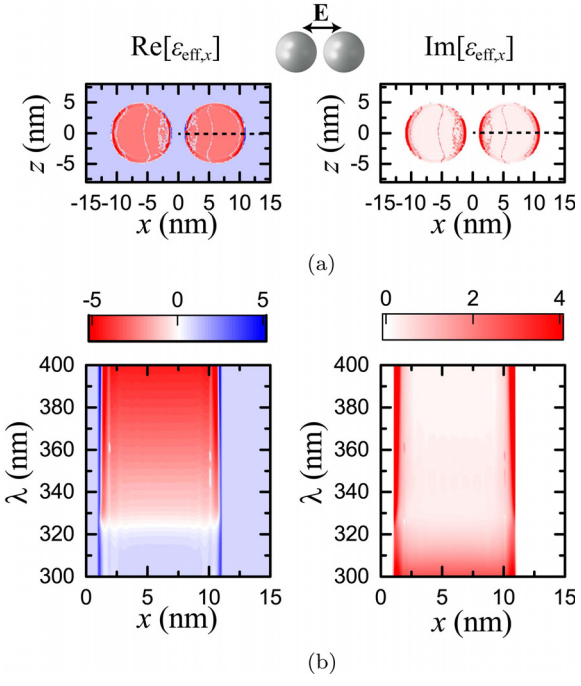

Fig. 5. (Color online) GNOR calculations for an Ag nanosphere dimer ($R = 5$ nm) separated by a 2-nm gap, illuminated by a plane wave polarized along the dimer axis (x-axis). (a) Real (left-hand contour) and imaginary (right-hand contour) part of the x component of the effective dielectric function, $\varepsilon_{\mathrm{eff},x}$, calculated at the resonant wavelength ($\lambda = 363$ nm) at a plane going through the middle of the particles. (b) Wavelength dependence of the real (left-hand contour) and imaginary (right-hand contour) part of $\varepsilon_{\mathrm{eff},x}$ along the dashed line in (a). Contour plots in (a) and (b) share common color scales.

a plane wave polarized along the dimer axis (taken to be the x-axis), as shown in the schematics. This dimer is characterized by the excitation of a bonding dimer plasmon, with its resonance at 363 nm. For the specific nanoparticle sizes and separations, nonlocal effects are expected to be important both because of the reduced size of the individual spheres and because of their narrow separation. In Fig. 5(a), we show the real (left-hand contour) and imaginary (right-hand contour) part of the x component of the effective dielectric function, retrieved within GNOR on resonance. Clearly, $\varepsilon_{\mathrm{eff},x}$ remains almost constant within the bulk of the particles, but large deviations occur near the interfaces, and the imaginary part obtains its largest values in a narrow region of a few Angstrom near the sphere boundaries, supporting again the picture of enhanced Landau damping as the main mechanism behind loss in small plasmonic systems. We note that additional small features inside the particles appear due to numerical instabilities owing to the increased meshing requirements in the finite-element method. In Fig. 5(b), we plot $\varepsilon_{\mathrm{eff},x}$ spectra for the same dimer, calculated along a line crossing the right-hand sphere at its middle, along the dashed lines of Fig. 5(a). The calculated dielectric

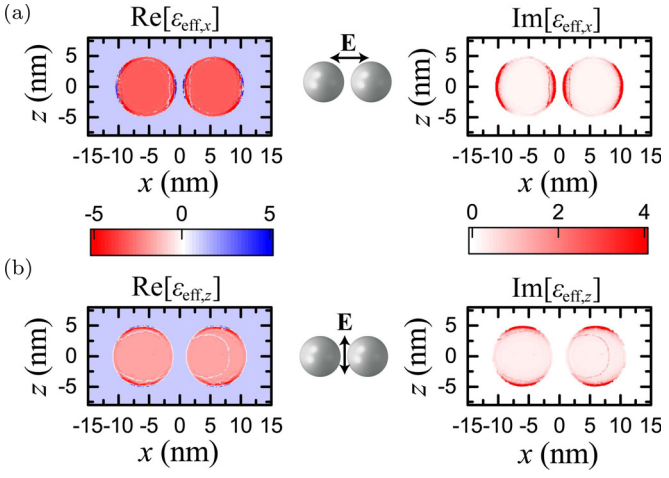

Fig. 6. (Color online) (a) Real (left-hand contour) and imaginary (right-hand contour) part of the x component of the effective dielectric function, $\varepsilon_{\mathrm{eff},x}$, calculated at the resonant wavelength ($\lambda = 373$ nm) for an Ag nanosphere dimer ($R = 5$ nm) separated by a 1-nm gap and illuminated by a plane wave polarized along the x-axis. (b) Real (left-hand contour) and imaginary (right-hand contour) part of the z component of the effective dielectric function, $\varepsilon_{\mathrm{eff},z}$, calculated at the resonant wavelength ($\lambda = 349$ nm) for an Ag nanosphere dimer ($R = 5$ nm) separated by a 2-nm gap and illuminated by a plane wave polarized along the z-axis. Contour plots in (a) and (b) share common color scales. All calculations are performed with the GNOR theory.

function follows well the experimental one[71] inside the bulk of the particles, with the real part changing sign at about 330 nm, and large nonlocal deviations only appear near the surfaces. It is also worth noting the behavior of the imaginary part, which is large near the surface for all wavelengths in agreement with our previous discussion, but becomes important also inside the particles for wavelengths shorter than 320 nm, where interband transitions dominate in silver.[4] Finally, we note that decreasing the gap increases the interaction between the spheres,[15] and this is accompanied by accordingly higher values of the imaginary part of the effective dielectric function near the surfaces, as shown in Fig. 6(a) for the dimer of Fig. 5 and a 1-nm gap. On the other hand, changing the polarization (taking for example **E** along the z-axis) leads to a charge accumulation in this direction at the two corresponding sides of the spheres, and Landau damping is mostly experienced there, as shown in Fig. 6(b) for a 2-nm-gap dimer.

5. Conclusion

In summary, we have discussed the origin of plasmon damping in flat metal–dielectric interfaces, small metallic nanoparticles and nanoparticle dimers, in view of the recent GNOR theory for nonlocal plasmonics. Through calculations of the effective dielectric function, using the GNOR model, a generalized Lindhard approach, or through *ab initio* TDDFT calculations, we have shown that in monomers, and in dimers with separations larger than a few Angstrom and/or a large metal work

function, plasmon damping and the corresponding modal broadening are adequately described by nonlocal convection–diffusion theory, which fully captures Landau damping near the metal surfaces.

Acknowledgments

C.T. was supported by funding from the People Programme (Marie Curie Actions) of the European Union's Seventh Framework Programme (FP7/2007-2013) under REA grant agreement number 609405 (COFUNDPostdocDTU). N.A.M. and M.W. gratefully acknowledge support from the VILLUM Fonden via the VKR Centre of Excellence NATEC-II and from the Danish Council for Independent Research (FNU 1323-00087). Center for Nanostructured Graphene (CNG) is financed by the Danish National Research Council (DNRF103). N.A.M. is a VILLUM Investigator supported by the VILLUM Fonden.

References

1. S. A. Maier, *Plasmonics: Fundamentals and Applications* (Springer, New York, 2007).
2. M. L. Brongersma, *Faraday Discuss.* **178**, 9 (2015).
3. A. Baev *et al.*, *Phys. Rep.* **594**, 1 (2015).
4. N. W. Ashcroft and N. D. Mermin, *Solid State Physics* (Saunders College, Fort Worth, 1976).
5. L. D. Landau, E. M. Lifshitz and L. P. Pitaevskii, *Electrodynamics of Continuous Media* (Butterworth Heinemann, Oxford, 1984).
6. S. I. Bozhevolnyi and N. A. Mortensen, *Nanophotonics* **6** (2017), doi:10.1515/nanoph-2016-0179.
7. W. Zhu *et al.*, *Nat. Commun.* **7**, 11495 (2016).
8. A. I. Fernández-Domínguez, F. J. García-Vidal and L. Martín-Moreno, *Nat. Photon.* **11**, 8 (2017).
9. S. I. Bozhevolnyi, L. Martín-Moreno and F. J. García-Vidal, *Quantum Plasmonics* (Springer International, New York, 2017).
10. D. K. Gramotnev and S. I. Bozhevolnyi, *Nat. Photon.* **4**, 83 (2010).
11. D. K. Gramotnev and S. I. Bozhevolnyi, *Nat. Photon.* **8**, 14 (2014).
12. L. M. Liz-Marzán, *Langmuir* **22**, 32 (2006).
13. E. Hao and G. C. Schatz, *J. Chem. Phys.* **120**, 357 (2004).
14. M. I. Stockman, *Phys. Rev. Lett.* **93**, 137404 (2004).
15. I. Romero *et al.*, *Opt. Express* **14**, 9988 (2006).
16. H. Duan *et al.*, *Nano Lett.* **12**, 1683 (2012).
17. A. Wiener *et al.*, *Nano Lett.* **12**, 3308 (2012).
18. F. J. García de Abajo, *J. Phys. Chem. C* **112**, 17983 (2008).
19. J. M. McMahon, S. K. Gray and G. C. Schatz, *Phys. Rev. Lett.* **103**, 097403 (2009).
20. C. David and F. J. García de Abajo, *J. Phys. Chem. C* **115**, 19470 (2011).
21. S. Raza *et al.*, *Phys. Rev. B* **84**, 121412(R) (2011).
22. J. Kern *et al.*, *Nano Lett.* **12**, 5504 (2012).
23. C. Ciracì *et al.*, *Science* **337**, 1072 (2012).
24. K. J. Savage *et al.*, *Nature* **491**, 574 (2012).
25. J. A. Scholl, A. L. Koh and J. A. Dionne, *Nature* **483**, 421 (2012).
26. S. Raza *et al.*, *Nanophotonics* **2**, 131 (2013).

27. S. Raza *et al.*, *Nat. Commun.* **5**, 4125 (2014).
28. S. F. Tan *et al.*, *Science* **343**, 1496 (2014).
29. D. Paria *et al.*, *Adv. Matter.* **27**, 1751 (2015).
30. S. Raza *et al.*, *Nat. Commun.* **6**, 8788 (2015).
31. H. Shen *et al.*, *Nano Lett.* **17**, 2234 (2017).
32. S. Raza *et al.*, *J. Phys., Condens. Matter* **27**, 183204 (2015).
33. G. Toscano *et al.*, *Opt. Express* **20**, 4176 (2012).
34. F. Bloch, *Z. Phys. A* **81**, 363 (1933).
35. R. Ruppin, *Phys. Rev. Lett.* **31**, 1434 (1973).
36. A. D. Boardman, *Electromagnetic Surface Modes. Hydrodynamic Theory of Plasmon-Polaritons on Plane Surfaces* (John Wiley and Sons, Chichester, 1982).
37. J. M. Pitarke *et al.*, *Rep. Prog. Phys.* **70**, 1 (2007).
38. N. A. Mortensen *et al.*, *Nat. Commun.* **5**, 3809 (2014).
39. A. V. Uskov *et al.*, *Plasmonics* **9**, 185 (2014).
40. J. B. Khurgin, *Faraday Discuss.* **178**, 109 (2015).
41. J. B. Khurgin and G. Sun, in *Springer Series in Solid-State Sciences 185: Quantum Plasmonics*, eds. S. I. Bozhevolniy *et al.* (Springer Nature, Cham, 2017), pp. 303–322.
42. W. Yan, M. Wubs and N. A. Mortensen, *Phys. Rev. Lett.* **115**, 137403 (2015).
43. G. Toscano *et al.*, *Nanophotonics* **2**, 161 (2013).
44. U. Kreibig and M. Vollmer, *Optical Properties of Metal Clusters* (Springer-Verlag, Berlin, 1995).
45. R. Esteban *et al.*, *Nat. Commun.* **3**, 825 (2012).
46. C. Tserkezis *et al.*, *Sci. Rep.* **6**, 28441 (2016).
47. J. A. Scholl *et al.*, *Nano Lett.* **13**, 564 (2013).
48. R. Esteban *et al.*, *Faraday Discuss.* **178**, 151 (2015).
49. U. Hohenester, *Phys. Rev. B* **91**, 205436 (2015).
50. S. Weiss *et al.*, *Phys. Status Solidi B* **188**, 343 (1995).
51. F. Benz *et al.*, *Opt. Express* **23**, 33255 (2015).
52. M. Grifoni and P. Hänggi, *Phys. Rep.* **304**, 229 (1998).
53. M. Büttiker, H. Thomas and A. Prêtre, *Phys. Lett. A* **180**, 364 (1995).
54. U. D. Keil *et al.*, *Appl. Phys. Lett.* **72**, 3074 (1998).
55. U. Hohenester and C. Draxl, *Phys. Rev. B* **94**, 165418 (2016).
56. A. Vagov *et al.*, *Phys. Rev. B* **93**, 195414 (2016).
57. T. V. Shahbazyan, *Phys. Rev. B* **93**, 235431 (2016).
58. X. Li, D. Xiao and Z. Zhang, *New J. Phys.* **15**, 023011 (2013).
59. D. Jin *et al.*, *Phys. Rev. Lett.* **115**, 193901 (2015).
60. P. J. Feibelman, *Prog. Surf. Sci.* **12**, 287 (1982).
61. T. Christensen *et al.*, *Phys. Rev. Lett.* **118**, 157402 (2017).
62. T. V. Teperik *et al.*, *Phys. Rev. Lett.* **110**, 263901 (2013).
63. T. V. Teperik *et al.*, *Opt. Express* **21**, 27306 (2013).
64. G. Toscano *et al.*, *Nat. Commun.* **6**, 7132 (2015).
65. W. Yan, *Phys. Rev. B* **91**, 115416 (2015).
66. C. Ciracì and F. Della Sala, *Phys. Rev. B* **93**, 205405 (2016).
67. Z. F. Öztürk *et al.*, *J. Nanophoton.* **5**, 051602 (2011).
68. J. B. Khurgin and G. Sun, *Opt. Express* **23**, 30730 (2015).
69. www.nanopl.org.
70. www.comsol.com.
71. P. B. Johnson and R. W. Christy, *Phys. Rev. B* **6**, 4370 (1972).